Theory for the hysteretic properties of the low-field dc magnetization in type-II superconductors

John R. Clem and Zhidong Hao*
Ames Laboratory and Department of Physics and Astronomy, Iowa State University, Ames, Iowa 50011
(Received 2 March 1993)

We examine theoretically the following types of magnetization measurements of type-II superconductors: (1) zero-field cooled (ZFC), (2) field cooled with data collected on cooling (FCC), (3) field cooled with data collected on warming (FCW), and (4) remanent. In analyzing the irreversible behavior of the low-field dc susceptibilities, the important parameters are the critical current density, sample dimensions, and lower critical field. We point out that the irreversibility temperature is determined by the merging point of the FCC and ZFC, but not the FCW and ZFC, magnetization curves.

I. INTRODUCTION

Following the discovery by Bednorz and Müller[1] of the onset of superconductivity in the Ba-La-Cu-O system above 30 K, as seen in the resistive transition, there have been numerous measurements of the magnetic susceptibility in related superconducting materials. The purpose of these investigations has been to confirm the existence of superconductivity at elevated temperatures, a large diamagnetic susceptibility being the characteristic signature. Two kinds of measurements have commonly been used. The first of these, often called a zero-field-cooled (ZFC) screening measurement, is performed by first cooling the sample in "zero" (or very small) magnetic field, applying a small (typically 0.1–100 Oe) field, and then measuring the resulting magnetization as a function of increasing temperature T using a sensitive magnetometer. The second kind of measurement, often called a field-cooled (FC) Meissner flux expulsion measurement, is performed by first applying a small (0.1–100 Oe) measuring field to a warm sample and then measuring the resulting magnetization versus T either upon decreasing the temperature or upon subsequently increasing it. In an ideal (pinning-free) simply connected bulk sample, in which the specimen always remains in thermodynamic equilibrium, the magnetization is exactly the same in either (ZFC or FC) experiment, simply the equilibrium magnetization corresponding to the given applied field and temperature. In nearly all real samples found in the laboratory, however, the two experiments yield different results, and it is the purpose of this paper to explain in detail why.

We begin by discussing the magnetization of high-temperature copper-oxide superconductors in increasing field but at constant temperature. Most bulk sintered samples of such materials are best described as granular superconductors, which consist of anisotropic superconducting grains that are Josephson coupled via intergranular weak links.[2] When a small magnetic field is applied, Josephson vortices are produced in the intergranular regions of the sample. The motion of these vortices is impeded by pinning forces arising from the inhomogeneity of the intergranular coupling energies, and the irreversible electrodynamics in this field regime is thus characterized by J_{cJ}, the critical-current density needed to depin a Josephson vortex. At higher magnetic fields, the intergranular regions become penetrated by a nearly uniform magnetic field associated with a densely packed array of overlapping intergranular Josephson vortices. As the field increases, vortices next penetrate into the superconducting grains. The motion of these vortices is also impeded by pinning forces, usually described by J_c, the intragranular critical-current density needed to depin a vortex. If the applied field is now reduced, magnetization hysteresis occurs, chiefly because of the irreversible nature of intragranular vortex motion.

When the temperature of the sample is varied in the presence of a constant applied magnetic field, similar effects occur, because both J_{cJ} and J_c depend upon the magnetic flux density B and temperature T. In the following, we analyze in detail how the magnetization changes as a function of temperature. For the present, however, we ignore the complications arising from the granular nature of the high-temperature superconductors and consider only monolithic superconductors in which flux pinning is characterized by a single critical-current-density function $J_c(B,T)$.[3–5] We also focus our attention upon the behavior of slab-shaped specimens in parallel applied fields. The treatment of the demagnetization effects for other specimen shapes should be straightforward using the physics described in this paper but will not be discussed here.

We already introduced in Refs. 6 and 7 some of the ideas on which this paper is based, and meanwhile closely related approaches have been used by several other authors[8–13] to explain much of the basic physics of the hysteretic dc magnetization. In the present paper we go beyond these previous works and provide a more complete theoretical framework for a detailed understanding of why different magnetic and thermal histories produce

different magnetization-versus-temperature curves.

In Sec. II we discuss the key concepts and introduce several model functions needed for computations. We also compute the magnetization versus increasing temperature for the zero-field-cooled (ZFC) screening case. In Sec. III we discuss and compute the magnetization for the case of field cooled with data collected on cooling (FCC), in which Meissner flux expulsion occurs under the influence of flux pinning. In Sec. IV we discuss and compute the magnetization for the case of field cooled with data collected on warming (FCW). In Sec. V we discuss and compute the remanent magnetization (RM), which is obtained by turning off the applied field after field cooling and then measuring as a function of increasing temperature. In Sec. VI we summarize our results and conclusions.

II. ZERO-FIELD-COOLED MAGNETIZATION

Consider a type-II superconducting slab of thickness D ($-D/2 < x < D/2$) initially cooled to low temperature in the absence of a magnetic field. Assume that, except very close to the transition temperature T_c, $D \gg \lambda(T)$, where $\lambda(T)$ is the temperature-dependent weak-field penetration depth. A parallel magnetic field H_0 is now applied, which obeys $H_0 < H_{c1}(0)$, where $H_{c1}(T)$ is the lower critical field at temperature T. Let T_{c1} and T_{c2} denote the temperatures at which H_0 is equal to H_{c1} and H_{c2}, respectively, where H_{c2} is the upper critical field. When $T < T_{c1}$, the specimen is in the Meissner state. Induced currents, flowing within λ of the surface, screen the bulk of the specimen from the applied field, such that the magnetic flux density B vanishes there and the magnetization M obeys $4\pi M/H_0 = -1$.

In the temperature range $T_{c1} < T < T_{c2}$ the specimen is in the mixed state, where magnetic flux enters the specimen in the form of quantized vortices. In the absence of pinning and surface barriers, the flux density B, averaged over the intervortex spacing, is uniform inside the specimen and equal to $B = B_{\rm eq}(H,T)$;[3–5] here $B_{\rm eq}(H,T)$ is the reversible flux density in equilibrium with a magnetic field H. Alternatively, we may say that B is given by the solution of $H_{\rm eq}(B,T) = H_0$; here $H_{\rm eq}(B,T) = 4\pi\partial F(B,T)/\partial B$, where $F(B,T)$ is the Helmholtz free energy density of the flux-line array.[14] The magnetization obeys $M = M_{\rm eq}$, where $M_{\rm eq}$ is simply the reversible equilibrium magnetization. For $T > T_{c2}$, bulk superconductivity is quenched, and, aside from weak paramagnetism or diamagnetism in the normal state, the magnetization is zero.

When pinning is present, however, the magnetization in the temperature range $T_{c1} < T < T_{c2}$ cannot achieve its equilibrium value. As T rises above T_{c1}, vortices are nucleated at the surfaces but are unable to move freely to produce uniform B in the specimen's interior. Instead, pinning forces tend to hold the vortices near the surfaces, building up a critical flux-density gradient there. According to the critical-state model[3–5] we have, neglecting flux creep,

$$|dH/dx| = (4\pi/c)J_c(B,T) \tag{1}$$

in the critical regions, which must be solved subject to the surface boundary condition $H = H_0$. The magnetization then is given by $-4\pi M = H_0 - \bar{B}$, where $\bar{B}$ is the volume average of B. As T increases, the profiles of $B(x,T)$ versus x change for two reasons: The difference between B and H at the surface [where $B = B_{\rm eq}(H_0,T)$, assuming no surface barriers] decreases, and the slope of B versus x [which is proportional to $J_c(B,T)$] decreases. The precise shape of the magnetization-versus-temperature curve depends upon the detailed dependences of $B_{\rm eq}(H,T)$ and $J_c(B,T)$ upon field and temperature.

To proceed further and do computations that illustrate the main features of the temperature dependence of the magnetization, we introduce several simple models. We approximate the temperature dependence of H_{c1} and H_{c2} by assuming the simple parabolic form, $H_{c1}(T)/H_{c1}(0) = H_{c2}(T)/H_{c2}(0) = 1 - t^2$, where $t = T/T_c$ is the reduced temperature. For the equilibrium B-vs-H relation [i.e., $B = B_{\rm eq}(H)$ or $H = H_{\rm eq}(B)$], although it is possible to treat the full problem numerically including the highly nonlinear behavior at low fields, we seek here a simpler approximation which enables analytic computations. For high-κ superconductors, such as the high-temperature superconductors (κ is the Ginzburg-Landau parameter), we choose the following approximation, which previously has been used in Ref. 6:

$$B_{\rm eq} = \begin{cases} 0, & H \le H_{c1} \\ H - fH_{c1}, & H > H_{c1} \end{cases}, \tag{2}$$

where $0 < f < 1$ is a dimensionless factor, and $H \ll H_{c2}$. This approximation, sketched in Fig. 1, idealizes the sharp rise in $B_{\rm eq}(H)$ at H just above H_{c1}. A similar model but with $f = 1$ has been used in Refs. 12 and 13. We neglect normal-state magnetism and fluctuation diamagnetism, and assume that $B = H$ in the normal state. It is known that the critical-current density $J_c(B,T)$ usually is a monotonically decreasing function of B. Since in this paper we restrict our attention to small applied fields $H_0 < H_{c1}(0)$, the resulting B inside the specimen obeys $B \ll H_{c2}$ except extremely close to T_c. We thus neglect the B dependence of J_c and take $J_c = J_c(T) = J_c(0,T)$. For the temperature dependence of J_c, we assume $J_c(T)/J_c(0) = [H_{c2}(T)/H_{c2}(0)]^n = (1-t^2)^n$, where $n \ge 1$. Experimentally it is found that n is typically in the range 1–3.[3] However, the above model for $J_c(T)$ ignores the possibility of the existence of a reversible region near T_c, where J_c is immeasurably small and the magnetization is practically reversible. We therefore propose

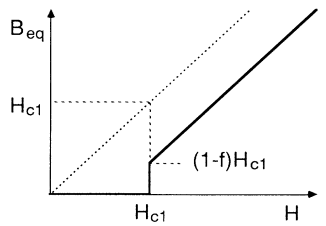

FIG. 1. Sketch of the model equilibrium B vs H behavior used for calculations in this paper.

the assumption

$$J_c = \begin{cases} J_c(0)(1-t^2/t_{\rm irr}^2)^n, & T \le T_{\rm irr} \\ 0, & T \ge T_{\rm irr}\ , \end{cases} \tag{3}$$

where $t_{\rm irr} = T_{\rm irr}/T_c$ and $T_{\rm irr}$ is the irreversibility temperature. For the body of this paper we treat the case $n = 1$ but discuss the behavior for $n > 1$ in the Appendix.

We also note that $H_{c2}/H_{c1} \gg 1$ in the high-temperature superconductors. Since we here consider only $H_0 < H_{c1}(0)$, it is easily shown that $T_{c2} \simeq T_c$, such that the difference between T_{c2} and T_c can be neglected.

We now compute the ZFC magnetization versus increasing temperature. Using Eq. (1) and the above models, we obtain the sequence of $B(x,T)$ profiles sketched in Fig. 2. Only $0 \le x \le D/2$ is shown because $B(-x,T) = B(x,T)$. For $T \le T_{c1}$ we have $B = 0$ [Fig. 2(a)]. For $T_{c1} < T < T_p$ the B profiles penetrate to the depth x_p [Fig. 2(b)]. The shoulderlike B-vs-x profile near x_p arises from the behavior near H_{c1} of the model $B_{\rm eq}(H)$ sketched in Fig. 1. For a more realistic model of $B_{\rm eq}(H)$, the penetrating B-vs-x profile would still rise sharply at x_p, but the shoulder would be rounded. At $T = T_p$ the flux front reaches the middle of the sample ($x = 0$) [Fig. 2(c)]. As T further increases, the slope of the $B(x,T)$ profile further decreases [Fig. 2(d)], eventually becoming perfectly flat at $T_{\rm irr}$. For $T \ge T_{\rm irr}$ the flux density is uniform [Fig. 2(e)], and for $T \ge T_c$ (we hereafter ignore the difference between T_{c2} and T_c) we have $B = H_0$ [Fig. 2(f)]. The $B(x,T)$ profiles are given explicitly by

$$B = H_0 - fH_{c1} + (4\pi/c)J_c(x - D/2) \tag{4}$$

for $x_p \le x \le D/2$ when $T_{c1} \le T \le T_p$, or for $0 \le x \le D/2$ when $T_p \le T \le T_c$ ($J_c = 0$ for $T \ge T_{\rm irr}$). The position x_p is determined by $H(x_p) = H_{c1}$ or $B(x_p) = H_{c1}(1-f)$. Since

$$x_p = D/2 - (H_0 - H_{c1})/(4\pi/c)J_c \tag{5}$$

is the depth to which the advancing B profile penetrates, the temperature T_p at which $x_p = 0$ is

$$T_p = T_{\rm irr}\left(\frac{\gamma + t_{c1}^2}{\gamma + t_{\rm irr}^2}\right)^{1/2}. \tag{6}$$

Here $t_{c1} = T_{c1}/T_c < 1$ and

$$\gamma = \frac{(4\pi/c)J_c(0)(D/2)}{H_{c1}(0)} \tag{7}$$

is a dimensionless measure of the pinning strength.

The magnetization computed from the above B profiles obeys

$$4\pi M/H_0 = -1, \quad T \le T_{c1}, \tag{8}$$

$$= -1 + \left[1 - \frac{(2f-1)(1-t^2)}{1-t_{c1}^2}\right]\frac{t^2 - t_{c1}^2}{2f\tilde{\gamma}(t_{\rm irr}^2 - t^2)}, \quad T_{c1} \le T \le T_p, \tag{9}$$

$$= -f\left[1 - t^2 + (\tilde{\gamma}/2)(t_{\rm irr}^2 - t^2)\right]/(1 - t_{c1}^2), \quad T_p \le T \le T_{\rm irr}, \tag{10}$$

$$= -f(1-t^2)/(1-t_{c1}^2), \quad T_{\rm irr} \le T \le T_c. \tag{11}$$

Here we have defined for convenience the quantity

$$\tilde{\gamma} = \gamma/ft_{\rm irr}^2. \tag{12}$$

In the absence of pinning Eq. (9) does not apply, since $T_p = T_{c1}$ and $\gamma = 0$. Calculated curves of the ZFC magnetization versus increasing temperature are shown in Fig. 3 for several values of $\tilde{\gamma}$ and the assumption that $f = 0.7$, $t_{c1} = 0.20$, and $t_{\rm irr} = 0.95$. Note that the magnetization changes slope discontinuously at T_p.

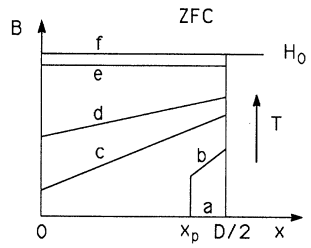

FIG. 2. ZFC profiles of $B(x,T)$ vs x for $\tilde{\gamma} = 2$ [Eq. (12)], $f = 0.7$, and (a) $0 \le T \le T_{c1}$, (b) $T_{c1} < T < T_p$, (c) $T = T_p$, (d) $T_p < T < T_{\rm irr}$, (e) $T_{\rm irr} < T < T_c$, and (f) $T \ge T_c$ for temperature increasing after zero-field cooling [see Eqs. (4)–(12)].

III. FIELD-COOLED MAGNETIZATION DURING COOLING

Consider next the case for which the sample is cooled through its superconducting transition temperature in a small parallel magnetic field H_0. As the temperature is reduced below T_c, magnetic flux is expelled from the

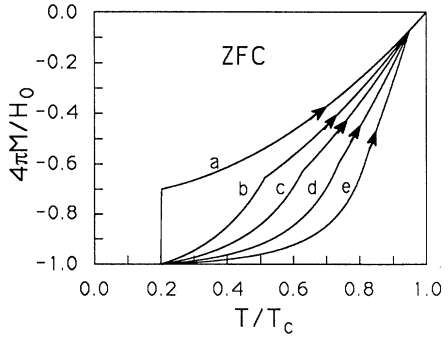

FIG. 3. ZFC magnetization vs increasing temperature in magnetic field H_0 after zero-field cooling, calculated from Eqs. (8)–(11) for $f = 0.7$, $T_{c1}/T_c = 0.20$, $T_{\rm irr}/T_c = 0.95$, and $\tilde{\gamma}$ [Eq. (12)] = (a) 0, (b) 0.5, (c) 1.0, (d) 2.0, and (e) 4.0. The corresponding values of T_p/T_c are (a) 0.20, (b) 0.51, (c) 0.63, (d) 0.74, and (e) 0.82.

sample, an effect often called Meissner flux expulsion. In the presence of pinning (for $T < T_{irr}$) the resulting magnetization obeys $-4\pi M = H_0 - \bar{B}$, but this quantity is smaller than the corresponding reversible magnetization $[-4\pi M = H_0 - B_{eq}(H_0, T)]$ because $\bar{B} > B_{eq}(H_0, T)$. It was found even upon discovery of the Meissner effect that some flux remained trapped upon cooling through T_c.[15] More recently, numerous studies related to practical applications of flux-trapping effects in various sample geometries have been carried out, starting with Refs. 16–19.

For weak pinning (sufficiently small values of J_c and γ), profiles of $B(x,T)$ vs x, from which the volume average $\bar{B}$ can be computed, are easily found from critical-state theory. Using the models of Sec. II, for example, we find

$$B(x,T) = H_0 - fH_{c1}(T)\ ,\ T_{irr} \le T \le T_c, \tag{13}$$

$$= H_0 - fH_{c1}(T) + (4\pi/c)J_c(T)(D/2 - x),\quad T_{c1} \le T \le T_{irr}, \tag{14}$$

$$= B(x, T_{c1}),\quad 0 \le T \le T_{c1}. \tag{15}$$

Note that the flux distribution freezes in at T_{c1}, where $B(D/2, T_{c1}) = 0$. The FCC magnetization versus temperature for weak pinning obeys

$$4\pi M/H_0 = -f(1-t^2)/(1-t_{c1}^2),\quad T_{irr} \le T \le T_c, \tag{16}$$

$$= -f\left[1 - t^2 - (\tilde{\gamma}/2)(t_{irr}^2 - t^2)\right]/(1-t_{c1}^2),\quad T_{c1} \le T \le T_{irr}, \tag{17}$$

$$= -f\left[1 - \tilde{\gamma}(t_{irr}^2 - t_{c1}^2)/2(1-t_{c1}^2)\right],\quad 0 \le T \le T_{c1}. \tag{18}$$

For strong pinning (sufficiently large values of J_c and γ), it is clear that something goes wrong with this simple calculation, because Eq. (14), for example, then yields $B(0,T) > H_0$ and $M > 0$. What is not included in these equations, however, is a careful treatment of flux trapping in the middle of the specimen (freezing-in of the magnetic flux distribution). We now show that, as the temperature decreases below T_{irr} to a temperature T, the critical-state theory can be used to calculate a characteristic flux-trapping depth[6] $L(T)$. As T decreases still further, the flux profile $B(x,T)$ changes within a distance $L(T)$ from the surface (so long as $T > T_{c1}$), but, at distances greater than $L(T)$ from the surface, the flux density remains frozen at the value it had upon freeze-in.

To calculate $L(T)$, assume decreasing temperature and consider two critical-state profiles [Eq. (14)], $B(x, T + \Delta T)$ and $B(x,T)$ vs x, at two successive temperatures, $T + \Delta T$ and T. For small ΔT the change in the flux density at x is

$$\Delta B(x,T) = B(x,T) - B(x, T+\Delta T), \tag{19}$$

$$= [f(dH_{c1}/dT) - (4\pi/c)(dJ_c/dT)(D/2 - x)]\Delta T. \tag{20}$$

At the surface $x = D/2$, $\Delta B(D/2, T) < 0$, since $dH_{c1}/dT < 0$. However, since we also have $dJ_c/dT < 0$, we see that $\Delta B = 0$ at $x = D/2 - L(T)$, where

$$L(T) = \frac{f(dH_{c1}/dT)}{(4\pi/c)(dJ_c/dT)}. \tag{21}$$

This quantity, which we call the flux-trapping depth, is the maximum depth at which B can change as the sample cools below temperature T. At distances farther than $L(T)$ from the surface, B is frozen in, because the magnitude of the corresponding gradient of H is less than the critical value for depinning [Eq. (1)]. When the exponent n for J_c (Sec. II) is larger than 1, $L(T)$ is a monotonically increasing function of T, diverging at T_{irr}. If, as the temperature decreases, $L(T)$ remains larger than $D/2$ until final freeze-in occurs at T_{c1}, the flux-density profiles and magnetization versus temperature remain as described in Eqs. (13)–(18). Otherwise, flux trapping changes the flux-density distribution near the center of the specimen, and the magnetization is modified accordingly.

To demonstrate the effects of flux trapping, we now consider the case for which $n = 1$, where n is the J_c exponent (Sec. II) (we consider the case of $n > 1$ in the Appendix). Using the models introduced in Sec. II, we find that for $n = 1$ the corresponding flux-trapping depth L is temperature independent:

$$L = \frac{ft_{irr}^2 H_{c1}(0)}{(4\pi/c)J_c(0)} = D/2\tilde{\gamma}. \tag{22}$$

When $\tilde{\gamma} \le 1$, we see that $L \ge D/2$, such that the results of Eqs. (13)–(18) remain valid at all temperatures. When $\tilde{\gamma} > 1$, on the other hand, $L < D/2$, and flux trapping begins as soon as the temperature drops below T_{irr}. Magnetic flux freezes in with constant density $B = B_{eq}(H_0, T_{irr})$ in the middle of the specimen $[0 \le x \le (D/2 - L)]$. However, the expressions Eqs. (14) and (15) remain valid for $(D/2 - L) \le x \le D/2$. In Fig. 4 we show the flux-density profiles for the case $L < D/2$. The magnetization now obeys

$$4\pi M/H_0 = -f(1-t^2)/(1-t_{c1}^2),\quad T_{irr} \le T \le T_c, \tag{23}$$

$$= -f\left[1 - t_{irr}^2 + (1/2\tilde{\gamma})(t_{irr}^2 - t^2)\right]/(1-t_{c1}^2),\quad T_{c1} \le T \le T_{irr}, \tag{24}$$

$$= -f\left[1 - t_{irr}^2 + (1/2\tilde{\gamma})(t_{irr}^2 - t_{c1}^2)\right]/(1-t_{c1}^2),\quad 0 \le T \le T_{c1}. \tag{25}$$

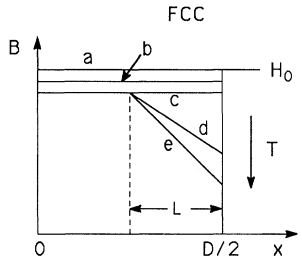

FIG. 4. FCC profiles of $B(x,T)$ vs x for strong pinning, $\tilde{\gamma} = 2$, $f = 0.7$, and (a) $T \geq T_c$, (b) $T_{\rm irr} < T < T_c$, (c) $T = T_{\rm irr}$, (d) $T_{c1} < T < T_{\rm irr}$, and (c) $0 \leq T \leq T_{c1}$, for field cooling in constant applied field with decreasing temperature. Flux is trapped with density $B = B_{\rm eq}(H_0, T_{\rm irr})$ in the region at depths greater than the flux-trapping depth L, here modeled as being temperature independent.

Figure 5 shows the calculated field-cooled magnetization during cooling (FCC) for several values of $\tilde{\gamma}$ [Eq. (12)] and the assumption that $f = 0.7$, $t_{c1} = 0.20$, and $t_{\rm irr} = 0.95$.

An important parameter to measure the effect of pinning is the Meissner fraction f_M, which is the ratio of FCC magnetization at $T \leq T_{c1}$ to the corresponding ZFC magnetization. The Meissner flux expulsion during cooling in constant applied field is never complete, except for the idealized case of zero pinning. Therefore f_M is always less than unity and decreases monotonically as a function of the low-field flux-pinning strength, as measured by the dimensionless parameter γ (or $\tilde{\gamma}$) when $n = 1$. For $n > 1$ the corresponding dimensionless parameter is the temperature-dependent quantity (see the Appendix)

$$\gamma(T) = n(4\pi/c)J_c(T)(D/2)/fH_{c1}(T). \qquad (26)$$

As shown in the Appendix, the ratio f_M is a function of γ_{c1}, the value of $\gamma(T)$ at T_{c1} when $H_{c1} = H_0$ and final freeze-in occurs.

Figure 6 shows the dependence of f_M upon γ_{c1} for several values of the exponent n, as calculated in the Appendix using the assumption $T_{c1} < T_{\rm irr} = T_c$. The sharp drop in f_M, from the value $f_M = 1$ in the absence of pinning to the value $f_M = f$ in the presence of very weak pinning, but with nonzero J_c ($\gamma_{c1} \to 0$), arises from the discontinuity at $H = H_{c1}$ in our simplified model for $B_{\rm eq}(H)$ [Fig. 1 and Eq. (2)]. This sharp drop would become more gradual if one were to perform numerical computations using a more accurate $B_{\rm eq}(H)$ relation. [For example, a good approximate $B_{\rm eq}(H)$, valid in the entire field region between H_{c1} and H_{c2}, is given in Ref. 20.] Since $\gamma(T)$ is proportional to the sample dimension D [Eq. (26)], we see that the Meissner fraction increases as the sample dimension decreases. Also note from Eq. (3) when $n > 1$ that J_c decreases with temperature more rapidly than H_{c1}, and $\gamma(T)$ [Eq. (26)] decreases as T increases; therefore, for smaller values of H_0 (higher values of T_{c1}), γ_{c1} becomes very small, and f_M is maximized. This is consistent with experimental observations, such as those of Ref. 8 and Ref. 21. Note that for a sufficiently small H_0, it may be possible to make $T_{c1} > T_{\rm irr}$; such a case would correspond to the absence of flux pinning, and our theory then would predict that $f_M \to 1$ for a realistic model in which $B_{\rm eq}(H)$ goes smoothly to zero as $H \to 0$.

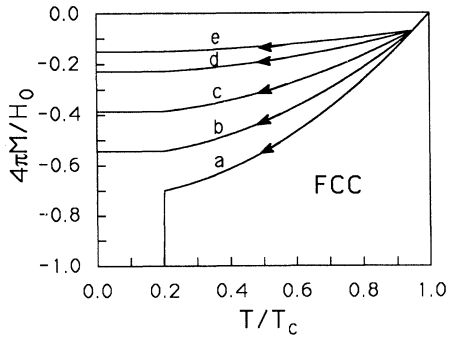

FIG. 5. FCC magnetization vs decreasing temperature during field cooling in field H_0, calculated from Eqs. (16)–(18) and (23)–(25) for $f = 0.7$, $T_{c1}/T_c = 0.20$, $T_{\rm irr}/T_c = 0.95$, and $\tilde{\gamma}$ = (a) 0, (b) 0.5, (c) 1.0, (d) 2.0, and (e) 4.0. The corresponding values of $L/(D/2)$ are ∞, 2.0, 1.0, 0.5, and 0.25.

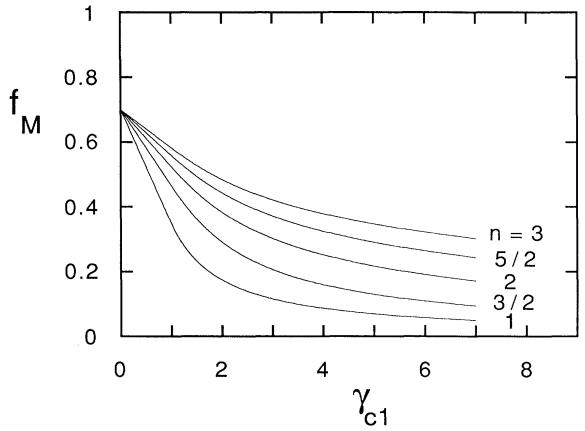

FIG. 6. The Meissner fraction f_M vs γ_{c1}, calculated in the Appendix [Eqs. (A12)–(A15)], for $f = 0.7$ and n =1, 3/2, 2, 5/2, and 3.

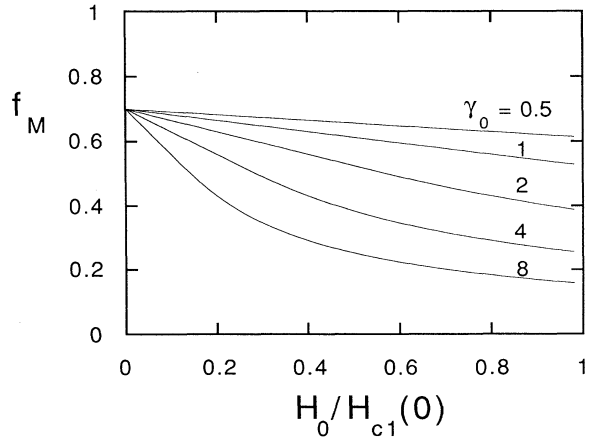

FIG. 7. The Meissner fraction f_M vs $H_0/H_{c1}(0)$, calculated in the Appendix, for $f = 0.7$, $n = 2$ [Eqs. (A12) and (A14)] and $\gamma_0 = \gamma(0)$ =0.5, 1, 2, 4, and 8.

Figure 7 shows the dependence of f_M upon $H_0/H_{c1}(0)$ for several values of $\gamma_0 = \gamma(0)$. The curves were calculated using the procedure described in the Appendix.

IV. FIELD-COOLED MAGNETIZATION DURING WARMING

Consider now the case for which the magnetization is measured during warming after the sample first has been cooled in a parallel applied field H_0. Since magnetic flux has been expelled in the initial field-cooling step, eventually a corresponding amount of flux must reenter the specimen. However, since magnetic flux moves down (but not up) a critical-state-density gradient, hysteresis occurs, and the warming magnetization does not retrace the cooling curve. The critical-state model again can be used to compute the resulting magnetization, but the details are more complex than might be expected.

We examine first the case of weak pinning (corresponding to $\tilde{\gamma} < 1$ for $n = 1$). For $0 \le T \le T_{c1}$ the flux distribution remains stationary, retaining the gradient established during field cooling [Eq. (15)]. For $T_{c1} < T < T_v$, however, $B(x,T)$ has a V-shaped minimum at $x = x_v$. For $x < x_v$, $dB(x,T)/dx = -(4\pi/c)J_c(T)$, while for $x > x_v$, $dB(x,T)/dx = +(4\pi/c)J_c(T)$. As the temperature increases, x_v decreases monotonically from its initial value ($x_v = D/2$) at T_{c1} to its final value ($x_v = 0$) at T_v. During this process, vortices on both sides of the minimum move down their respective critical-state-density gradients, which are now less steep than they were at temperatures $T \le T_{c1}$. To the right of x_v, vortices move to the left, while to the left of x_v, vortices move to the right. At x_v the vortex velocity and the vortex-motion-induced electric field are zero, and this condition yields an equation of motion for x_v, which can be solved to determine x_v and the corresponding profiles of $B(x,T)$ as functions of T over the temperature interval $T_{c1} \le T \le T_v$.

When the J_c exponent obeys $n = 1$, the weak-pinning case corresponds to $\tilde{\gamma} \le 1$ (or $L > D/2$). The equation of motion for x_v for this case is found as follows. When $T_{c1} \le T \le T_v$, the flux-density profile obeys

$$B = H_0 - fH_{c1} + (4\pi/c)J_c(x - D/2), \quad x_v \le x \le D/2, \tag{27}$$

$$= H_0 - fH_{c1} - (4\pi/c)J_c(D/2 + x - 2x_v), \quad 0 \le x \le x_v. \tag{28}$$

We first obtain an expression for the electric field in the region $0 \le x \le x_v$ by taking the time derivative of Eq. (28) and applying Faraday's law. The requirement that the electric field be zero at x_v leads to the equation

$$2(4\pi/c)J_c x_v' = fH_{c1}' - (4\pi/c)J_c'(3x_v/2 - D/2), \tag{29}$$

where the prime denotes differentiation with respect to temperature T. With the help of the models introduced in Sec. II with $n = 1$, we obtain

$$\tilde{x}_v = \frac{2}{3\tilde{\gamma}}\left[1 + \tilde{\gamma} - (1 - \tilde{\gamma}/2)\left(\frac{t_{\rm irr}^2 - t_{c1}^2}{t_{\rm irr}^2 - t^2}\right)^{3/4}\right], \quad T_{c1} \le T \le T_v, \tag{30}$$

where $\tilde{x}_v = 2x_v/D$. The V-shaped minimum in the B profiles reaches the center of the specimen at the temperature

$$T_v = T_{\rm irr}\left[1 - (1 - t_{c1}^2/t_{\rm irr}^2)\left(\frac{1 - \tilde{\gamma}/2}{1 + \tilde{\gamma}}\right)^{4/3}\right]^{1/2}, \quad (\tilde{\gamma} \le 1)\ . \tag{31}$$

For $T_v \le T \le T_{\rm irr}$ the B profiles are given by Eq. (27).

For $\tilde{\gamma} \le 1$ the magnetization computed from Eqs. (27)–(31) obeys

$$4\pi M/H_0 = -f\left[1 - \tilde{\gamma}(t_{\rm irr}^2 - t^2)/2(1 - t_{c1}^2)\right], \quad 0 \le T \le T_{c1}, \tag{32}$$

$$= -f\left[1 - t^2 - \tilde{\gamma}(t_{\rm irr}^2 - t^2)(\tilde{x}_v^2 - 1/2)\right]/(1 - t_{c1}^2), \quad T_{c1} \le T \le T_v, \tag{33}$$

$$= -f\left[1 - t^2 + (\tilde{\gamma}/2)(t_{\rm irr}^2 - t^2)\right]/(1 - t_{c1}^2), \quad T_v \le T \le T_{\rm irr}, \tag{34}$$

$$= -f(1 - t^2)/(1 - t_{c1}^2), \quad T_{\rm irr} \le T \le T_c. \tag{35}$$

For the strong-pinning case ($\tilde{\gamma} > 1$) the time evolution of the flux-density profiles is a little more complicated, because the initial profile for $0 \le T \le T_{c1}$, Fig. 8(a), is not that of Eq. (27) but that of Fig. 4(e),

$$B = H_0 - fH_{c1}(T_{\rm irr}), \quad 0 \le x \le D/2 - L, \tag{36}$$

$$= (1 - f)H_0 + (4\pi/c)J_c(T_{c1})(D/2 - x), \quad (D/2 - L) \le x \le D/2. \tag{37}$$

For $T_{c1} < T < T_f$ the flux-disturbance region, as shown in Fig. 8(b), penetrates only to x_f, while flux remains trapped at density $B(T_{\rm irr}) = H_0 - fH_{c1}(T_{\rm irr})$ in the region $0 \le x \le x_f$. A V-shaped minimum occurs at x_v. In the region $x_f < x < x_v$ vortices move down the critical-state-density gradient to the right, and in the region $x_v < x \le D/2$ vortices similarly move to the left. The critical-state-density gradient becomes less steep as the temperature rises. The $B(x,T)$ profiles are given explicitly by

$$B = H_0 - fH_{c1}(T_{\rm irr}), \quad 0 \le x \le x_f, \tag{38}$$

$$= H_0 - fH_{c1} - (4\pi/c)J_c(x - 2x_v + D/2), \quad x_f \le x \le x_v, \tag{39}$$

$$= H_0 - fH_{c1} + (4\pi/c)J_c(x - D/2), \quad x_v \le x \le D/2. \tag{40}$$

By again applying Faraday's law, requiring the electric

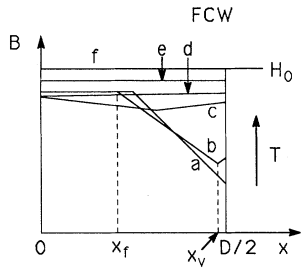

FIG. 8. FCW profiles of $B(x,T)$ vs x for strong pinning, $\tilde{\gamma}=2$, $f=0.7$, and (a) $0 \le T \le T_{c1}$, (b) $T_{c1} < T < T_f$, (c) $T_f < T < T_v$, (d) $T_v < T < T_{irr}$, (e) $T_{irr} < T < T_c$, and (f) $T \ge T_c$ for temperature increasing after initial field cooling [Eqs. (36)–(45)].

field to be zero at x_v, and solving the resulting differential equation for x_v, we obtain

$$\tilde{x}_v = 1 + 1/\tilde{\gamma} - (1/\tilde{\gamma})\left(\frac{t_{irr}^2 - t_{c1}^2}{t_{irr}^2 - t^2}\right)^{1/4}, \tag{41}$$

$$\tilde{x}_f = 2\tilde{x}_v - 1 - 1/\tilde{\gamma}, \tag{42}$$

where $\tilde{x}_f = 2x_f/D$.

The temperature T_f at which x_f reaches the center of the specimen ($x_f = 0$) is

$$T_f = T_{irr}\left[1 - \frac{16(1 - t_{c1}^2/t_{irr}^2)}{(1+\tilde{\gamma})^4}\right]^{1/2}. \tag{43}$$

For $T_f < T < T_v$, Eq. (41) no longer applies, but the situation [Fig. 8(c)] becomes similar to that for $\tilde{\gamma} \le 1$. Equation (29) again applies but must be solved subject to the initial condition, $\tilde{x}_{v1} = (1 + 1/\tilde{\gamma})/2$, where $\tilde{x}_{v1}$ is the value of $\tilde{x}_v$ at T_f. The solution is

$$\tilde{x}_v = \frac{2}{3\tilde{\gamma}}\left[1 + \tilde{\gamma} - \frac{2}{(1+\tilde{\gamma})^2}\left(\frac{t_{irr}^2 - t_{c1}^2}{t_{irr}^2 - t^2}\right)^{3/4}\right]. \tag{44}$$

The temperature T_v at which x_v reaches the center of the specimen ($x_v = 0$) is

$$T_v = T_{irr}\left[1 - \frac{2^{4/3}(1 - t_{c1}^2/t_{irr}^2)}{(1+\tilde{\gamma})^4}\right]^{1/2} \quad (\tilde{\gamma} \ge 1). \tag{45}$$

For $T_v < T < T_{irr}$ [Fig. 8(d)] the B profiles are again given by Eq. (27).

The magnetization for $\tilde{\gamma} \ge 1$ is therefore

$$4\pi M/H_0 = -f\left[1 - t_{irr}^2 + (1/2\tilde{\gamma})(t_{irr}^2 - t_{c1}^2)\right]/(1 - t_{c1}^2), \quad 0 \le T \le T_{c1}, \tag{46}$$

$$= -f\left[1 - t^2 + (\tilde{\gamma}/2)(t_{irr}^2 - t^2)(1 + \tilde{x}_f^2 - 2\tilde{x}_v^2)\right]/(1 - t_{c1}^2), \quad T_{c1} \le T \le T_f, \tag{47}$$

$$= -f\left[1 - t^2 + (\tilde{\gamma}/2)(t_{irr}^2 - t^2)(1 - 2\tilde{x}_v^2)\right]/(1 - t_{c1}^2), \quad T_f \le T \le T_v, \tag{48}$$

$$= -f\left[1 - t^2 + (\tilde{\gamma}/2)(t_{irr}^2 - t^2)\right]/(1 - t_{c1}^2), \quad T_v \le T \le T_{irr}, \tag{49}$$

$$= -f(1 - t^2)/(1 - t_{c1}^2), \quad T_{irr} \le T \le T_c. \tag{50}$$

Figure 9 exhibits the calculated curves of the field-cooled magnetization during warming (FCW) for several values of $\tilde{\gamma}$ and the assumption that $f = 0.7$, $t_{c1} = 0.20$, and $t_{irr} = 0.95$.

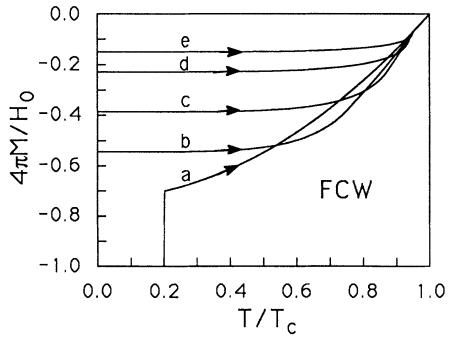

FIG. 9. FCW magnetization vs increasing temperature after initial field cooling in field H_0, calculated from Eqs. (32)–(35) and (46)–(50) for $f = 0.7$, $T_{c1}/T_c = 0.20$, $T_{irr}/T_c = 0.95$, and $\tilde{\gamma} =$ (a) 0, (b) 0.5, (c) 1.0, (d) 2.0, and (e) 4.0.

V. REMANANT MAGNETIZATION

Finally, we consider the case for which the applied field H_0 is turned off after the specimen is field cooled to below T_{c1} and the remanent magnetization (RM) is measured as a function of increasing temperature.

We examine first the case of weak pinning (corresponding to $\tilde{\gamma} < 1$ for $n = 1$). For $0 \le T \le T_{c1}$, the flux distribution remains unchanged as established during field cooling. Here we consider a long slab specimen, so that demagnetization effects can be neglected, and we also neglect flux-creep effects. As T is increased above T_{c1}, the $B(x,T)$ profiles change because $B(D/2,T) = (1-f)H_{c1}(T)$ at the surface decreases, and the slope of B vs x [which is proportional to $J_c(T)$] decreases. The flux-density profile obeys

$$B = (1 - f)H_{c1} - (4\pi - /c)J_c(x - D/2). \tag{51}$$

Using the models of Sec. II with $n = 1$, the magnetization $4\pi M = \bar{B}$ for $\tilde{\gamma} < 1$ computed from the above equation obeys

$$4\pi M/H_0 = 1 - f + f\tilde{\gamma}(t_{\rm irr}^2 - t_{\rm c1}^2)/2(1 - t_{\rm c1}^2), \quad 0 \le T \le T_{\rm c1}, \tag{52}$$
$$= \left[(1-f)(1-t^2) + (f\tilde{\gamma}/2)(t_{\rm irr}^2 - t^2)\right]/(1 - t_{\rm c1}^2), \quad T_{\rm c1} \le T < T_{\rm irr}, \tag{53}$$
$$= 0, \quad T_{\rm irr} \le T. \tag{54}$$

The flux-density distribution $B(x,T)$ and the magnetization collapse suddenly at $T = T_{\rm irr}$, the temperature above which pinning is ineffective.[6]

For the case of strong pinning ($\tilde{\gamma} > 1$) the profiles of $B(x,T)$ vs x follow the sequence shown in Fig. 10. For $0 \le T \le T_{\rm c1}$ [Fig. 10(a)] the $B(x,T)$ profile is given by Eqs. (36) and (37). For $T_{\rm c1} < T < T_f$ the flux-disturbance region, as shown in Fig. 10(b), is $x_f \le x \le D/2$, while flux remains trapped at density $H_0 - fH_{\rm c1}(T_{\rm irr})$ in the region $0 \le x < x_f$. The $B(x,T)$ profile is given explicitly by

$$B = H_0 - fH_{\rm c1}(T_{\rm irr}), \quad 0 \le x < x_f, \tag{55}$$
$$= (1-f)H_{\rm c1} - (4\pi/c)J_c(x - D/2), \quad x_f \le x \le D/2, \tag{56}$$

where

$$\tilde{x}_f = 2x_f/D = 1 - 1/\tilde{\gamma} - (t^2 - t_{\rm c1}^2)/f\tilde{\gamma}(t_{\rm irr}^2 - t^2). \tag{57}$$

The temperature T_f at which x_f reaches the center of the specimen ($x_f = 0$) [Fig. 10(c)] is

$$T_f = T_{\rm irr}\left[\frac{f(\tilde{\gamma}-1) + t_{\rm c1}^2/t_{\rm irr}^2}{f(\tilde{\gamma}-1)+1}\right]^{1/2}. \tag{58}$$

For $T_f \le T < T_{\rm irr}$, the $B(x,T)$ profile is given by Eq. (56) [Fig. 10(d)].

The magnetization for $\tilde{\gamma} \ge 1$ is therefore

$$4\pi M/H_0 = 1 - f\left[1 - t_{\rm irr}^2 + (1/2\tilde{\gamma})(t_{\rm irr}^2 - t_{\rm c1}^2)\right]/(1 - t_{\rm c1}^2), \quad 0 \le T \le T_{\rm c1}, \tag{59}$$
$$= \left[(1-f)(1-t^2) + (f\tilde{\gamma}/2)(t_{\rm irr}^2 - t^2)(1-\tilde{x}_f^2)\right]/(1-t_{\rm c1}^2), \quad T_{\rm c1} \le T \le T_f, \tag{60}$$
$$= \left[(1-f)(1-t^2) + (f\tilde{\gamma}/2)(t_{\rm irr}^2 - t^2)\right]/(1-t_{\rm c1}^2), \quad T_f \le T < T_{\rm irr}, \tag{61}$$
$$= 0, \quad T_{\rm irr} \le T \le T_c. \tag{62}$$

Again the flux-density distribution $B(x,T)$ and the magnetization collapse suddenly at $T = T_{\rm irr}$.

Figure 11 exhibits the calculated remanent magnetization (RM) for several values of $\tilde{\gamma}$ and the assumption that $f = 0.7$, $t_{\rm c1} = 0.20$, and $t_{\rm irr} = 0.95$. The discontinuity in $M(T)$ at $T = T_{\rm irr}$ arises from the discontinuity in our model for $B_{\rm eq}(H,T)$ [Fig. 1 and Eq. (2)].

Shown in Fig. 12 are the expected ZFC, FCC, FCW, and RM magnetization-versus-temperature curves. Because the flux-density profiles are frozen in at temperatures below $T_{\rm c1}$, the magnetization versus temperature is flat in this temperature range. In the temperature range $T_{\rm c1} < T < T_{\rm irr}$, where $J_c > 0$, the critical-state model requires that the FCC magnetization curve (which describes a flux density that has negative slope near the surface, as in Fig. 4) must lie above the FCW magnetization curve (which describes a flux density that has positive slope near the surface, as in Fig. 8). This hysteretic nature of the magnetization versus temperature, as shown by the FCC and FCW curves in Fig. 12, has been confirmed by the recent experiments of Deak *et al.*[22] and Hyun.[23] Only when J_c is effectively zero, i.e., only when $T > T_{\rm irr}$, is the flux-density profile flat. For such temperatures, the flux-density profiles for ZFC, FCC, and FCW all agree, and one is then measuring simply the reversible

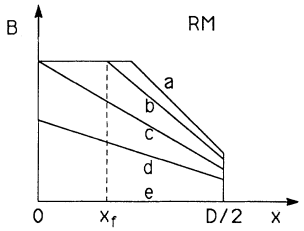

FIG. 10. RM profiles of $B(x,T)$ vs x for $\tilde{\gamma} = 2$, $f = 0.7$, and (a) $0 \le T \le T_{\rm c1}$, (b) $T_{\rm c1} < T < T_f$, (c) $T = T_f$, (d) $T_f < T < T_{\rm irr}$, and (e) $T \ge T_{\rm irr}$ [Eqs. (55)–(58)].

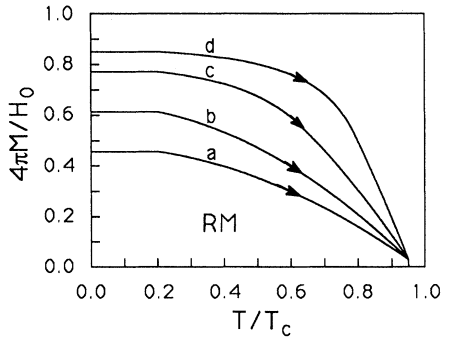

FIG. 11. RM magnetization vs increasing temperature after initial field cooling in field H_0 and then turning off H_0, calculated from Eqs. (52)–(54) and (59)–(62) for $f = 0.7$, $T_{\rm c1}/T_c = 0.20$, $T_{\rm irr}/T_c = 0.95$, and $\tilde{\gamma}$ = (a) 0.5, (b) 1.0, (c) 2.0, and (d) 4.0.

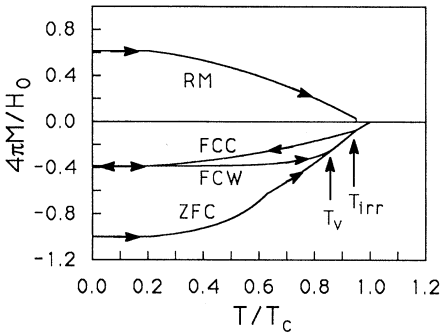

FIG. 12. Calculated ZFC, FCC, FCW, and RM magnetization vs temperature for $\tilde{\gamma} = 1$, $f = 0.7$, $T_{c1}/T_c = 0.20$, and $T_{irr}/T_c = 0.95$.

(equilibrium) magnetization curve. The RM magnetization is zero in the reversible region, since, in contrast to the ZFC, FCC, and FCW cases, the applied field is zero.

It is easy to see that $M_{RM} = M_{FCC} - M_{ZFC}$ for $T \leq T_{c1}$. This property has been pointed out previously in Ref. 6 and has been confirmed experimentally.[24] However, it is important to notice that the relation $M_{RM} = M_{FCC} - M_{ZFC}$ holds only for $T \leq T_{c1}$. For $T > T_{c1}$, although the remanent magnetization M_{RM} resembles the difference between M_{FCC} and M_{ZFC}, a detailed comparison shows that there is *not*, in principle, an exact equality between M_{RM} and $M_{FCC} - M_{ZFC}$.

Note that the flux-density profiles for ZFC and FCW are identical for $T \geq T_v$ [Figs. 2(c), 2(d), 2(e), and 2(f), and Figs. 8(d), 8(e), and 8(f)]. Thus the magnetization curves for the two processes must be identical for $T \geq T_v$. It is clear, however, that T_v in principle has nothing to do with the irreversibility temperature T_{irr}, since the joining of the two magnetization curves at T_v (which is below T_{irr}) follows from the critical-state model, which is describing the irreversibility of the sample.

VI. SUMMARY

Using the critical-state model, we have considered theoretically the following types of low-field dc magnetization of type-II superconductors: (1) zero-field-cooled magnetization (ZFC), (2) field-cooled magnetization with data collected on cooling (FCC), (3) field-cooled magnetization with data collected on warming (FCW), and (4) remanent magnetization (RM).

In agreement with the approaches of Refs. 8–13, we find that in analyzing these magnetization measurements, the most important factors are the critical-current density, the sample dimension, and the equilibrium properties of the sample as described by the relation $B = B_{eq}(H)$. We have performed model calculations to demonstrate the influence of these factors on the temperature dependences of the above four types of magnetization measurements and the Meissner fraction f_M.

An important feature revealed by the theory is that the irreversibility temperature T_{irr} is determined by the merging point of the ZFC and FCC (or FCC and FCW), but not by the ZFC and FCW magnetization curves.

ACKNOWLEDGMENTS

Ames Laboratory is operated for the U.S. Department of Energy by Iowa State University under Contract No. W-7405-Eng-82. This work was supported in part by the Director for Energy Research, Office of Basic Energy Sciences.

APPENDIX

In this appendix we consider the magnetic flux-density profiles $B(x,T)$ vs x during field cooling for the general case that the flux trapping depth L is T dependent. We also consider the Meissner fraction for such a case.

Since here we are interested in the temperature region below the irreversibility temperature T_{irr}, for simplicity we set $T_{irr} = T_c$ in Eq. (3); i.e.,

$$J_c(T) = J_c(0)(1-t^2)^n. \tag{A1}$$

The dimensionless parameter measuring the pinning strength is

$$\gamma(T) = \frac{n(4\pi/c)J_c(T)(D/2)}{fH_{c1}(T)} \tag{A2}$$

$$= \gamma(0)(1-t^2)^{n-1}, \tag{A3}$$

and the flux-trapping depth [Eq. (21)] is

$$L(T) = \frac{L(0)}{(1-t^2)^{n-1}} = D/2\gamma(T). \tag{A4}$$

Here both $\gamma(T)$ and $L(T)$ are T dependent for $n > 1$. When temperature is lowered, $\gamma(T)$ increases and $L(T)$ decreases. Final freeze-in of the flux-density distribution occurs at $T_{c1} = T_c[1 - H_0/H_{c1}(0)]^{1/2}$.

If $\gamma_{c1} = \gamma(T_{c1}) < 1$ [Eq. (A3)], then $L_{c1} = L(T_{c1}) > D/2$ [Eq. (A4)], and the flux-density profiles are given at all temperatures between T_{c1} and T by

$$B = H_0 - fH_{c1} - (4\pi/c)J_c(x - D/2). \tag{A5}$$

On the other hand, if $\gamma_{c1} = \gamma(T_{c1}) > 1$ so that $L_{c1} = L(T_{c1}) < D/2$, there is a temperature $T_0 > T_{c1}$ at which $L = D/2$. As T is lowered below T_0, $L(T)$ becomes less than $D/2$, so that flux is trapped in the region $0 \leq x \leq D/2 - L(T)$. The expression for the flux-density profile in the flux-trapping region for $n > 1$ can be found as follows. Suppose the flux-density profile at point x ceases changing at temperature T_x ($T_{c1} \leq T_x \leq T_0$). Then

$$L(T_x) = D/2 - x \tag{A6}$$

$$= L(0)/(1-t_x^2)^{n-1}, \tag{A7}$$

$$1 - t_x^2 = \left[\frac{L(0)}{D/2 - x}\right]^{1/(n-1)}. \tag{A8}$$

The flux-density profile at the point x is no longer a function of T for $T \leq T_x$ but is given by

$$B(x) = H_0 - fH_{c1}(T_x) - (4\pi/c)J_c(T_x)(x - D/2) \tag{A9}$$

$$= H_0\left\{1 - \frac{f(n-1)}{n[\gamma_{c1}(1-\tilde{x})]^{1/(n-1)}}\right\}, \tag{A10}$$

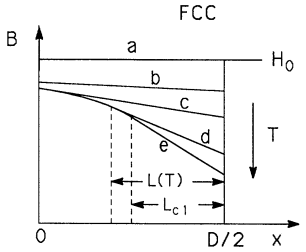

FIG. 13. FCC profiles of $B(x,T)$ vs x for $n = 2$, $\gamma_{c1} = 2$, $f = 0.7$, and (a) $T \geq T_c$, (b) $T_0 < T < T_c$, (c) $T = T_0$, (d) $T_{c1} < T < T_0$, and (e) $0 \leq T \leq T_{c1}$, for field cooling in constant applied field with decreasing temperature [Eqs. (A5) and (A10)].

where we have used Eq. (A8). Equation (A10) holds for $0 \leq x \leq D/2 - L(T)$. The flux-density profile in the region $D/2 - L(T) \leq x \leq D/2$ is linear and given by Eq. (A5). Figure 13 shows, for example, a sequence of flux-density profiles during field cooling, calculated from Eqs. (A5) and (A10), for $n = 2$, $f = 0.7$, and $\gamma_{c1} = 2$.

The Meissner fraction f_M, which is the ratio of the field-cooled magnetization at $T \leq T_{c1}$ to the corresponding zero-field-cooled magnetization, can be expressed as

$$f_M = -4\pi M(T_{c1})/H_0 \,, \tag{A11}$$

where $M(T_{c1})$ is the field-cooled magnetization at T_{c1}; f_M can be calculated from the freeze-in flux-density profile, $B(x,T_{c1})$ [Eqs. (A5) and (A10)]. We find for $\gamma_{c1} \leq 1$ that

$$f_M = f\,(1 - \gamma_{c1}/2n)\,, \tag{A12}$$

and for $\gamma_{c1} \geq 1$

$$f_M = f/2\gamma_{c1} \quad (n = 1), \tag{A13}$$

$$= f\,(3/2 + \ln\gamma_{c1})\,/2\gamma_{c1} \quad (n = 2), \tag{A14}$$

$$= \frac{f}{2(2-n)\gamma_{c1}}\left[1 - \frac{2(n-1)^2}{n}\gamma_{c1}^{(n-2)/(n-1)}\right] \quad (n > 1, n \neq 2). \tag{A15}$$

Figure 6 shows f_M vs γ_{c1}, calculated from Eqs. (A12)–(A15), for several values of n and $f = 0.7$. Figure 7 shows f_M vs $H_0/H_{c1}(0)$, calculated from Eqs. (A12) and (A14), for $n = 2$, $f = 0.7$, and several values of $\gamma_0 = \gamma(0)$.

*Present address: Texas Center for Superconductivity, University of Houston, Houston, Texas 77204.

[1] J. G. Bednorz and K. A. Müller, Z. Phys. **64**, 189 (1986).
[2] J. R. Clem, Physica C **153-155**, 50 (1988).
[3] A. M. Campbell and J. E. Evetts, Adv. Phys. **21**, 199 (1972).
[4] H. Ullmaier, *Irreversible Properties of Type-II Superconductors* (Springer, Berlin, 1975).
[5] J. R. Clem, J. Appl. Phys. **50**, 3518 (1979).
[6] L. Krusin-Elbaum, A. P. Malozemoff, D. C. Cronemeyer, F. Holtzberg, J. R. Clem, and Z. Hao, J. Appl. Phys. **67**, 4670 (1990).
[7] L. Krusin-Elbaum, A. P. Malozemoff, D. C. Cronemeyer, F. Holtzberg, G. V. Chandrashekhar, J. R. Clem, and Z. Hao, Physica A **168**, 367 (1990).
[8] K. Kitazawa, O. Nakamura, T. Matsushita, Y. Tomioka, N. Motohira, M. Murakami, and H. Takei, in *Advances in Superconductivity II*, edited by T. Ishiguro and K. Kajimura (Springer-Verlag, Tokyo, 1990).
[9] T. Matsushita, E. S. Otabe, T. Matsumoto, M. Murakami, and K. Kitazawa, Physica C **170**, 375 (1990).
[10] K. Kitazawa, T. Matsushita, O. Nakamura, Y. Tomioka, N. Motohira, T. Tamura, T. Hasegawa, K. Kishio, I. Tanaka, and H. Kojima, in *International Conference on Superconductivity-ICSC, Bangalore, India*, edited by S. K. Joshi, C. N. R. Rao, and S. V. Subramanyam (World Scientific, Singapore, 1990), p. 241.
[11] K. Tomioka, Y. Nakayama, M. Naito, T. Matsushita, I. Tanaka, H. Kojima, T. Ishii, K. Kishio, K. Yamafuji, and K. Kitazawa, Physica C **185-189**, 2163 (1991).
[12] V. V. Moshchalkov, A. A. Zhukov, V. D. Kuznetsov, V. V. Metlushko, V. I. Voronkova, and B. K. Yanovskii, Solid State Commun. **74**, 1295 (1990).
[13] V. V. Moshchalkov and A. A. Zhukov, Physica B **169**, 601 (1991).
[14] A. L. Fetter and P. C. Hohenberg, in *Superconductivity*, edited by R. D. Parks (Marcel Dekker, New York, 1969).
[15] W. Meissner and R. Ochsenfeld, Naturwissenschaften **21**, 787 (1933).
[16] C. P. Bean and M. V. Doyle, J. Appl. Phys. **33**, 3334 (1962).
[17] D. L. Coffey, W. F. Gauster, and A. E. Rorschach, Jr., Appl. Phys. Lett. **3**, 75 (1963).
[18] D. G. Schweitzer, Phys. Lett. **34A**, 220 (1971).
[19] M. Rabinowitz, E. L. Garwin, and D. J. Frankel, Lett. Nuovo Cimento **7**, 1 (1973).
[20] Z. Hao, J. R. Clem, M. W. McElfresh, L. Civale, A. P. Malozemoff, and F. Holtzberg, Phys. Rev. B **43**, 2844 (1991).
[21] L. Krusin-Elbaum, A. P. Malozemoff, Y. Yeshurun, D. C. Cronemeyer, and F. Holtzberg, Physica C **153**, 1469 (1988).
[22] J. Deak, M. McElfresh, J. R. Clem, Z. Hao, M. Konczykowski, R. Muenchausen, S. Foltyn, and R. Dye, Phys. Rev. B **47**, 8377 (1993); (unpublished).
[23] O. B. Hyun, Physica C **206**, 169 (1993); Phys. Rev. B **48**, 1244 (1993).
[24] L. Krusin-Elbaum, A. P. Malozemoff, and G. V. Chandrasekhar, Physica C **162-164**, 1553 (1989).